The design of a slit ICRF antenna in EU-DEMO

Fusion Engineering and Design 189 (2023) 113453

Contents lists available at ScienceDirect

Fusion Engineering and Design

journal homepage: www.elsevier.com/locate/fusengdes

The design of a slit ICRF antenna in EU-DEMO

H. Kasahara [a,*], K. Saito [a,b], T. Seki [a], T. Mutoh [c]

[a] National Institute for Fusion Science, National Institutes of Natural Sciences, Toki, Gifu 509-5292, Japan
[b] SOKENDAI, The Graduate University for Advanced Studies, Toki, Gifu 509-5292, Japan
[c] Chubu University, Kasugai-shi, Aichi 487-8501, Japan

ARTICLE INFO

Keywords:
ICRF heating
ICRF antenna
High power density
Electric field
DEMO
Reactor

ABSTRACT

Although ICRF heating has achieved the high heating efficiency necessary to achieve high-performance plasmas, it has not overcome the reliability and economic problems associated with the antenna structure inside the vacuum vessel in fusion reactors. We suggested a slit ICRF antenna that uses the blanket surface as a transmission line to solve these problems. With a single slit ICRF antenna with a width of 3 m and a height of 15 cm, the electric field strength to the magnetic field direction was successfully suppressed to 5 kV/cm when 20 MW of power radiation was achieved from the single slit. The slit ICRF antenna had a bending angle in the electromagnetic wave transmission path to prevent direct neutron impact on the first wall and a vacuum gate from rapidly preventing water or air leakage accidents. The slit ICRF antenna has a simple structure that allows heating at high power density while minimizing blanket volume reduction.

1. Introduction

An ion Cyclotron range of frequencies (ICRF) heating is one of the attractive methods to heat high-density plasmas exceeding 10^{20} m^{-3} with high heating efficiency [1] and to drive plasma-current [2] with controlling current phase on strap surfaces for ICRF antennas. Fast ion production with large triple products, high heating efficiency [3], and impurity control [4,5] were demonstrated using ICRF waves.

On an ICRF antenna in European DEMO (EU-DEMO) [6], a loop type ICRF antenna [7,8] and a traveling wave antenna (TWA) [9] is suggested, and their structure is designed based on the traditional experiment knowledge for ICRF heating experiments with the large antenna–plasma coupling [10]. In traditional ICRF antenna experiments, mitigating RF sheath effects related to local heat loads is one of the critical issues, and the RF sheath may cause impurity generations and increase neutral particles around ICRF antennas. These effects increase the possibility of breaking down between the antenna strap, the Faraday screen, or the protectors.

We hope to decrease the RF sheath effect by optimizing the current profile on the strap surfaces and reducing the parallel electric field ($E_{\|}$) to the magnetic field line. A field-aligned ICRF antenna has been developed to make ideal wave excitation with a negligible $E_{\|}$ in the Large Helical Device (LHD) [11], and Alcator C-Mod [12]. They successfully reduced impurity production and local heat loads during ICRF heating. As the other method of RF sheath reduction, current profile optimization with a multi-strap ICRF antenna has been challenged in the ASDEX-U [13], and it showed the reduction of $E_{\|}$ from the finite element method (FEM) calculation. These studies indicated that ICRF heating could reduce parasitic heating related to RF sheath to control the current profile on the straps. However, several issues in designing an ICRF antenna remain, and they are associated with the antenna geometry inside the vacuum vessel in reactors. The loop-type ICRF antennas have a complex antenna structure, which increases assembly and maintenance costs and, as with all equipment with cooling systems in vacuum vessels, reduces reliability due to the risk of water leakage.

A waveguide ICRF antenna is one of the candidates to solve these issues, but the waveguide size is large (~ 3 m on the frequency of 50 MHz) in recent large-size devices for fusion plasma experiments, respectively. To challenge designing a waveguide ICRF antenna to excite a mode-converted ion Bernstein wave in the LHD, a folded waveguide antenna experiment was conducted [14]. In order to shorten the length of the long axis of the rectangular waveguide, the waveguide is folded in a truncated shape, resulting in a compact waveguide antenna. In this experiment, the waveguide antenna was installed just in front of an X-point of the divertor leg, and a large amount of wave power went to divertor plates through the divertor leg. This issue was strongly related to the installation issues, and there is no suggestion that waveguide antennas cannot excite electromagnetic waves more suitable for heating than loop-type antennas.

The DEMO and reactor are large enough to encapsulate a waveguide ICRF antenna within the vacuum vessel and blanket module, making a waveguide ICRF antenna in DEMO feasible. This paper shows a design

* Corresponding author.
E-mail address: kasahara.hiroshi@nifs.ac.jp (H. Kasahara).

https://doi.org/10.1016/j.fusengdes.2023.113453
Received 1 October 2022; Received in revised form 3 January 2023; Accepted 12 January 2023
Available online 26 January 2023

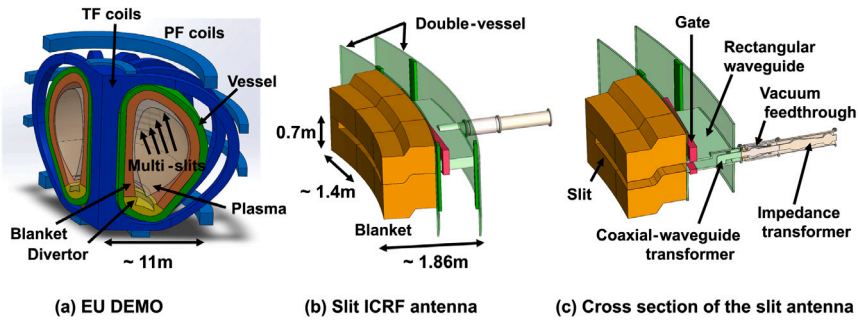

Fig. 1. Overview of a slit ICRF antenna in EU-DEMO.

of a slit ICRF antenna as a waveguide antenna for ICRF heating and an overview of the slit ICRF antenna based on the EU-DEMO. Second, we discuss the critical parameters and capability of exciting wave power using the single slit ICRF antenna with a simple antenna model using the commercial finite element method (FEM), COMSOL [15]. Finally, we suggested the design values of a single slit ICRF antenna and discussed the remaining research issues for the slit ICRF antenna.

2. Overview of a slit ICRF antenna in EU-DEMO

Fig. 1 shows the overview of the design for a multi-slit ICRF antenna in EU-DEMO (a), an overview of the single slit ICRF antenna component connected to the external coaxial line (b), and the cross-section for the single slit ICRF antenna (c). As a design for a waveguide ICRF antenna, the slit ICRF antenna consists of five key components, a slit waveguide on the blanket surface, a vacuum gate in the rectangular waveguide, a transducer from the coaxial line to the rectangular waveguide, vacuum feedthrough connected to the external coaxial line, and the coaxial line with impedance transformer such as Fig. 1(c). The components of slit ICRF antennas have simple structures, and they could share with the elementary component for the EU-DEMO and reactors. For neutron impact damage, their components are not critical compared with the other components in the vacuum vessel, and there are no differences in reliability between with or without the slit ICRF antenna in reactors. We suggest these slit surfaces, on which ICRF wave propagates, are covered by tungsten like the surface of a blanket face to plasma to reduce Joule loss from the wave propagation. In fusion reactors, the reduction of neutron shielding due to the installation of heating and measurement equipment is an important issue. This slit antenna is expected to mitigate the reduction of neutron shielding due to the decreasing blanket volume by achieving high power density excitation for the single slit ICRF antenna. In excited power density for a single slit ICRF antenna, we discuss the capability in the next section using a simple wave propagation model on the slit surface. For the other vital components, the vacuum feedthrough and impedance transformer have been developed in long-pulse plasma operation in the LHD, and a duration time of 48 min with a heating power of 1.2 MW was achieved with good reliability. At the LHD, the heating power is much less than at EU-DEMO, but the critical voltage of the coaxial system regarding electrical design can be increased by scaling up the coaxial line diameter with the increase in incident power based on the experience of the long-pulse ICRF heating in the LHD. Of course, mechanical and thermal structure optimization will be necessary due to scale-up, but significant structural redesigns will not be required. Empirically, transmission lines with coaxial structures for high power transmission can be designed as efficiently in EU-DEMO as in existing methods.

3. Capability of injection power in the single slit ICRF antenna

To effectively excite electromagnetic waves from the blanket surface, a simplified rectangular waveguide propagation model for EU-DEMO (Fig. 2) was used to predict the propagation and reflection of electromagnetic waves in the slit ICRF antenna and the electric field strength on the slit at the blanket surface. The design values of the slit antenna model include the transmission distance L from the vacuum vessel to the blanket, the bending angle *theta* in the center of the blanket, the length *height* in the short axis direction, and *width* in the long axis direction of the slit on the blanket surface, the fillet radius R to reduce the electric field concentration due to convexity in the slit, and the overlap thickness t in the linear direction for neutron shielding in blankets to prevent direct impact on the first wall by neutrons. The locations R = 3.29 m, 9.44 m, 10.04 m, and 12.04 m correspond to the blanket surface near the center stack in the vacuum vessel, the blanket surface from which the electromagnetic waves of the slit ICRF antenna are excited, the inner wall surface of the double vacuum vessel, and the outer wall surface of the double vacuum vessel. Since the ICRF heating frequency currently used in EU-DEMO is planned to be 50 MHz, this slit ICRF antenna was also designed to be able to propagate electromagnetic waves at 50 MHz. As shown in Fig. 2, the model had no plasma region and had a uniform structure in the direction perpendicular to the horizontal plane except for the slit where the electromagnetic waves propagated. To investigate the propagation characteristics of electromagnetic waves in the slit antenna, an RF wave was launched from point B, the end of the rectangular waveguide, in Fig. 2(A), and the reflection coefficients, S_{11}, were calculated in various waveguide parameters. The wave power propagated into the slit antenna, some wave power was radiated from the slit antenna into the vacuum region at the blanket surface, and some wave power returned to the incident port B. Finally, wave power went to X_1 or X_2 for the radiation boundary in Fig. 2(A) or returned to injection port B.

The simplified wave propagation model revealed the effect of each parameter for the slit ICRF antenna. In this model, where there was no absorption of electromagnetic waves in the vacuum region, the electromagnetic waves radiated from the slit ICRF antenna were strongly reflective on the inner blanket surface, and the reflected waves might return to the slit that radiated the electromagnetic waves. The electric field strength at the slit surface was evaluated, including the effect of this composite reflection wave. Realistically, the curvature of the plasma surface just in front of the blanket and the propagation in the plasma is expected to reduce this reflected wave of electromagnetic waves back to the slit. Furthermore, since wave power in the actual plasma can be absorbed by the plasma on the propagation in the plasma, the reflected wave to the slit would be decreased than in the model, and the electric field strength at the slit aperture with this model would be overestimated.

To investigate the propagation characteristics of electromagnetic waves in the slit antenna, the reflection coefficient S_{11} of electromagnetic waves converted to a rectangular waveguide mode at R = 9.44 m could be used to investigate the exciting capability of electromagnetic waves at the blanket surface after conversion to waveguide mode. The RF launching port was set to point B in Fig. 2, and the output port of the wave was set to the sides of both toroidal vacuum regions. The launching port was the end of the rectangular waveguide, and the other boundaries were reflection boundaries as perfect conductors.

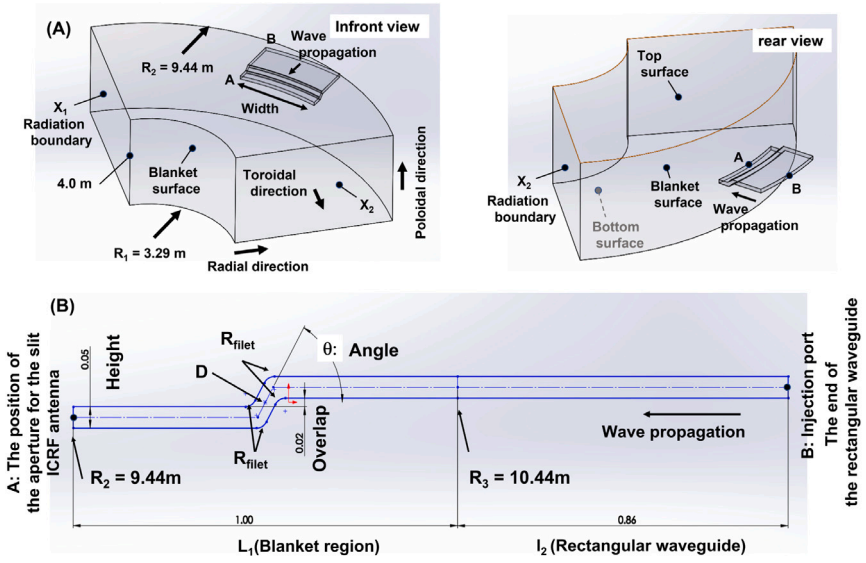

Fig. 2. A simple wave propagation model for the single slit ICRF antenna.

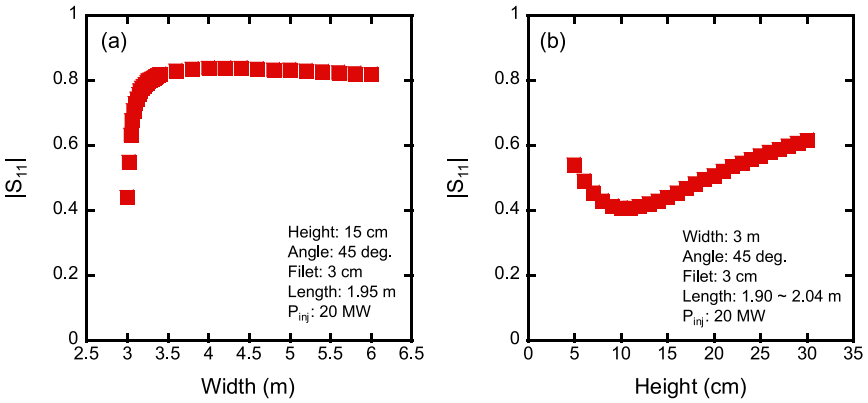

Fig. 3. Reflection coefficient S_{11} in various height and width of the waveguide aperture.

Note that even if S_{11} was zero, the electromagnetic wave incident from the coaxial line was not excited into the plasma without reflection, but there was a significant reflection by the coaxial waveguide converter. Coaxial waveguide conversion without cavity resonance generally exhibited low impedance at the conversion section, so the matching mechanism by impedance conversion was essential, but in this paper, the optimization method of impedance transducers [16] is out of scope.

In Fig. 3(a), when the width of the slit aperture became longer than the cutoff length of 3 m for electromagnetic waves of frequency 50 MHz, electromagnetic waves could propagate into the slit, and the S_{11} increased rapidly as the aperture width increased. Then, when the slit aperture length increased to 4.2 m, S_{11} reached a maximum and decreased gradually. To optimize the exciting power density of electromagnetic waves and mitigate the reduction of the blanket volume by the slit ICRF antenna, we suggested that *width* be 3 m, the same as the cutoff length. If the actual slit width is designed to be precisely 3 m, the propagation characteristics of electromagnetic waves in the slit will be significantly degraded if the slit is shorter than 3 m due to errors caused by installation, etc. Therefore, in actual design width, the width of the slit aperture should be designed as a few centimeters longer than the cutoff length at which electromagnetic waves can propagate.

Once the slit width was determined, which was the critical design value of the slit antenna, it was crucial to optimize the electric field strength on the slit aperture at the blanket surface. Increasing the height of the slit aperture decreased the electric field strength at the aperture, but it led to an increase in the aperture surface and a decrease in the tritium breeding volume of the blanket. The dependence on the aperture height with the slit width of 3 m according to Fig. 3(b) showed that the optimum value concerning S_{11} was at the height of 10 cm. The height at which S_{11} increased by about 10% from the optimum value was found to be between 8 cm and 15 cm, and a realistic slit height with reduced electric field strength was between 10 cm and 15 cm. Since the electric field strength decreased inversely proportional to height, 15 cm was chosen as a candidate height for the slit ICRF antenna to suppress the electric field strength to enable power excitation with a single-slit ICRF antenna as much as possible.

The power density and electric field strength distribution at the slit aperture when the slit width was 3 m, the aperture height was 15 cm, and the injection power was 20 MW were shown in Fig. 4. The average exciting power density from the antenna was 44.4 MW/m^2, but from Fig. 4(a), the maximum power density reached 93.7 MW/m^2 at the center of the slit aperture. In the slit ICRF antenna, electromagnetic waves were not evenly radiated from the slit aperture but were mainly concentrated near the center, with a power density distribution that decreased parabolically toward both ends of the slit's long axis direction. However, in the center of the short axis slit direction, the power density distribution was high at both ends and relatively low in the center. The radiated power density distribution of electromagnetic waves from the slit antenna could be considered in a similar way to the loop-type antenna because the distance from the center of the strap corresponds

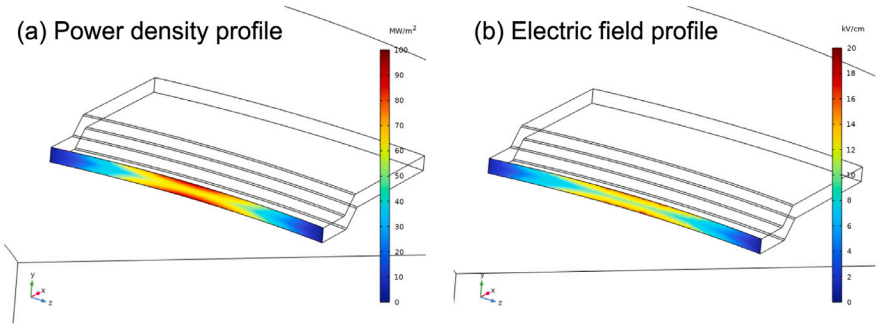

Fig. 4. Power density (a) and electric field (b) strength on the blanket surface for the slit ICRF antenna with the height of 15 cm and the width of 3 m.

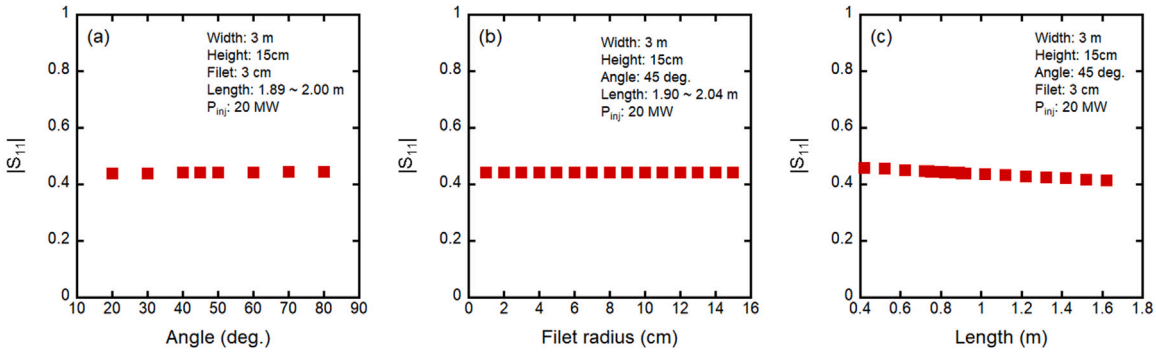

Fig. 5. Reflection coefficient S_{11} for the bending angle θ, and the filet radius R, and the length of propagation path L.

to the distance from the center of the slit aperture, and the propagation of electromagnetic waves after radiation could be considered in the same way. Like the power density, the electric field strength at the slit aperture was also more significant in the center and negligible at both ends of the aperture, and the electric field strength was mainly dominated by the component in the direction of the short axis of the slit.

Fig. 5 showed the dependence on the angle that bends the propagation path of the electromagnetic wave between the vacuum vessel wall and the blanket surface, the rounding radius R of the convexity that occurred at that time, and the resonance effect by varying the transmission path length of the vacuum section. Since the angle and the rounding radius R had a weak effect on the reflection coefficient S_{11}, it was sufficient to choose an angle that simplified the structure and increased reliability, and its radius R should be as large as possible to weaken the electric field. On the other hand, as for the dependence on the length inside the vacuum vessel, extending the transmission path improved the reflection coefficient slightly, but the transmission path became more complicated to increase the length inside the vessel, which reduced the system's reliability. Therefore, it was essential to choose the transmission path of the slit antenna with the shortest path for reliability and cost considerations.

Fig. 6 showed the electric field distribution of the perpendicular ($E_{\perp}$) and parallel ($E_{\parallel}$) direction to the magnetic field lines when the incident power was 20 MW, and the horizontal angle of the magnetic field at the front of the blanket surface was 15 degrees. The ICRF slit antenna had a width of 3 m, a height of 15 cm, transmission line curvature of 45 degrees, a fillet radius of 10 cm, and an overlap distance of 1 cm to prevent direct neutron impact on the first wall. The perpendicular electric field strength distribution had the same magnitude as the top and the bottom sections, with the maximum slightly shifted to the left and right compared to the maximum in the center, but the difference was negligible, such as Fig. 6(a). The parallel electric field strength had the same direction in the top and the bottom sections, but these positions of the maximum value were shifted by about 1 m. Since 20 MW of the electromagnetic wave was injected, the magnitude of the vertical electric field was 12.5 kV/cm, but the parallel electric field was below 5.0 kV/cm, and the direction of the parallel electric field was the same in the top and bottom sections. Therefore, as the single slit ICRF antenna, there was still enough margin for the injection power capability compared to the empirically obtained operation electric field strength of 15 kV/cm [17] with the magnetic field direction without arcing and damage.

Fig. 7 showed the results of the maximum electric field for parallel direction to the magnetic field lines at the blanket surface in various incident power and aperture heights. The reflection coefficient in Fig. 3 suggested that the reflection coefficient was minimum at 10 cm, but on the other hand, the electric field strength would be higher due to the shorter short-axis length. When the angle between the magnetic field at the blanket surface and the slit was 15 degrees, the parallel electric fields were less than 15 kV/cm even when the incident power was 40 MW if the slit height was 10 cm or higher. Since reliable ICRF heating prevents arcing and other damage with the parallel electric field of 15 kV/cm, the maximum operating electric field strength should be set at 10 kV/cm, which was smaller than the parallel electric field strength of 15 kV/cm. The maximum power of electromagnetic radiation was 22.1 MW at 10 cm height, 30.2 MW at 13 cm height, and more than 40 MW at 15 cm and 17 cm height. The angle with the magnetic field was set at 15 degrees, but it might increase to 20 degrees depending on the situation, so a height of at least 13 cm was necessary. We also proposed a minimum slit height of 15 cm, assuming higher inter-slit coupling due to the operation of multiple slits. The average power radiation density at the aperture was 51.3 MW/m^2 at a slit height of 13 cm, 64.4 MW/m^2 at 15 cm, and 39.2 MW/m^2 at 17 cm, ensuring that the slit antenna had a power radiation density of at least 30 MW/m^2 at any slit height It could be regarded as an ICRF antenna. Based on the above, EU-DEMO finally proposed the design values shown in Table 1 for the slit ICRF antenna with a slit height of 15 cm, which had a permitting parallel electric field and a small slit area.

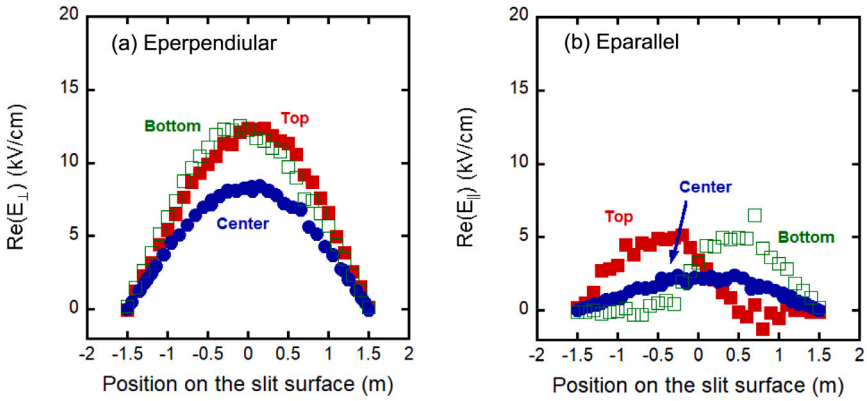

Fig. 6. Parallel (a) and perpendicular (b) electric fields on the three positions on the slit aperture at the blanket surface for the slit ICRF antenna with the assumption of magnetic angle in front of a blanket of 15°.

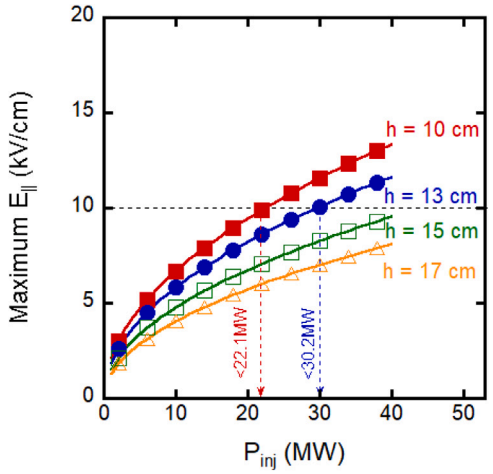

Fig. 7. Maximum of parallel electric fields on the single slit aperture for the blanket surface in various heights.

Table 1
The design parameters of a single-slit ICRF antenna in EU-DEMO.

Width	Height	Angle	Filet radius	Overlap thickness	P_{max}
3 m	0.15 m	45°	10 cm	1 cm	29 MW

4. Conclusion and discussion

Table 1 showed an example of the slit ICRF antenna in EU-DEMO. The aperture surface of the single slit ICRF antenna was 0.45 m^2 with the injection power of 20 MW, and a power density of 44 MW/m^2 was possible. The maximum electric field strength was approximately 12.5 kV/cm, and the parallel electric field to the magnetic field lines was 5.0 kV/cm, assuming an angle of 15 degrees with the magnetic field.

The slit ICRF antenna consists of five key components: a waveguide on a blanket surface, a vacuum gate in a rectangular waveguide, a coaxial line to a rectangular waveguide converter, vacuum feedthrough connecting to an external coaxial line, and an impedance converter. The propagation route of electromagnetic waves near the blanket in the vacuum vessel, which is particularly essential, uses the blanket surface, so the transmission path is realized by creating a simple shape on the blanket surface without a particular structure as an ICRF antenna. The slit ICRF antenna can be considered a very reliable and low-cost heating device because it has the capability of high power density radiated into the plasma, has a gate for vacuum closure inside the double vacuum vessel, and does not require special equipment for ICRF heating device except shared blankets in the vacuum vessel. In the impact of neutron breeding rate using the slit ICRF antenna, this slit antenna is designed to keep the blanket volume, not to decrease it by setting a waveguide. However, we must consider the neutron breeding rate, including the indirect interaction between the neutron and blanket module. The neutron analysis of the slit ICRF antenna is one of the future tasks to estimate the neutron breeding rate accurately.

On the other hand, in the current drive with multi-slit ICRF antennas, the study of electromagnetic excitation related to the increased reflectivity of the slit antenna due to the accurate magnetic field structure associated with the dielectric constant of the plasma has not yet been completed. In the initial calculation result of wave excitation with the multi-slit ICRF antenna on the plasma surface with the monotonical dielectric tensor, $\epsilon_r \sim 81$, the electric field was focused on the plasma surface in front of the slits with the vertical discrepancy between slits of 70 cm and the horizontal discrepancy between the slit centers of 38 cm such as Fig. 1(a). The geometrical expectation of an exciting parallel wavenumber is 7.9 m^{-1} with the angle of the magnetic file of 16° However, we must use a plasma model to evaluate the actual exciting spectrum in the plasma for the slit ICRF antenna, which is ongoing work. Especially in the case of simultaneous excitation by multiple slits, it is expected that the coupling between slits will be significant, and therefore plasma modeling studies are essential.

Although the TWA antenna is the most advantageous of the loop ICRF antennas in the EU-DEMO, it is not appropriate to compare the TWA with the slit ICRF antenna at the moment. The slit ICRF antenna determines the maximum available power from the electric field in the direction parallel to the magnetic field, while the TWA antenna determines the maximum available power from the maximum voltage of the antenna. This does not allow a fair evaluation of the radiated power density, which is important in the EU-DEMO for maintaining the blanket region. The TWA is designed for 50 MW injection with four ports in the toroidal direction and a radiated power density of 2.0–2.7 MW/m^2 with a maximum strap voltage of 30 kV. On the other hand, the slit ICRF antenna is assumed to inject 10–20 MW with one slit with a maximum parallel electric field below 10 kV/cm. Although it varies depending on the conditions, the breakdown voltage under vacuum is about 20 kV at 1 mm. The arc voltage of a loop-type ICRF antenna is usually the shortest distance between the current conductor and the Faraday shield. Considering that the breakdown voltage increases with the square root of the distance, the breakdown voltage is 63.2 kV when the shortest distance is about 1 cm. In an electromagnetic analysis of antennas, the electric field strength around the Faraday shield reaches 20–30 kV/cm. However, it has been reported that arcing occurs when the electric field strength in the direction parallel to the magnetic field reaches 18 kV/cm [17]. It is possible to apply the electric field strength of 30 kV/cm or more in the direction perpendicular to the magnetic field with the parallel electric field below 18 kV/cm. Since the injectable power of a TWA antenna can be improved simply by

taking the above into account, the currently evaluated radiated power density underestimates the actual performance that is possible. For these reasons, we would like to compare the TWA and the slit antennas after improving the TWA and getting the detail of the geometry of the TWA.

For the simulation of electromagnetic excitation, including plasma modeling, it is essential to determine the plasma parameters and design them simultaneously with the modular structure of the blanket. At this time, the details of the magnetic and blanket structures have not yet been determined, and simulations related to optimization, etc., are the subject of future research. Since slit ICRF antennas can also be realized in helical [18] and stellarator [19] fusion reactors with complex magnetic field structures, further research on blanket magnetic field structures for ICRF slit antennas is desirable.

CRediT authorship contribution statement

H. Kasahara: Conceptualization, Methodology, Software, Validation, Data curation, Formal analysis, Writing – original draft, Writing – review & editing. **K. Saito:** Methodology, Validation, Investigation, Data curation, Formal analysis. **T. Seki:** Methodology, Investigation, Formal analysis. **T. Mutoh:** Investigation, Data curation, Formal analysis.

Declaration of competing interest

The authors declare the following financial interests/personal relationships which may be considered as potential competing interests: H. Kasahara, K. Saito, T. Seki reports financial support was provided by National Institute for Fusion Science.

Data availability

Data will be made available on request.

Acknowledgments

We thank G.Nomura and M.Kanda for their help in preliminary studies and mock-up tests of the ICRF heating system. This work was supported by the National Institute for Fusion Science grant management budget, Japan (NIFS19ULR703, NIFS20ULR703, and NIFS21ULR703), for which computational resources were prepared and implemented.

References

[1] R. Bilato, V. Bobkov, A. Kappatou, R. McDermott, T. Odstril, G. Tardini, M. Bernert, R. Dux, M. Maraschek, J.-M. Noterdaeme, F. Ryter, J. Stoberand, M. Nocente, T. Hellsten, P. Mantica, M. Tardocchi, S.K. Nielsen, J. Rasmussen, M. Stejner, et al., Bulk ion heating with ICRF waves in tokamaks, AIP Conf. Proc. 1689 (1) (2015).

[2] Y. Kazakov, D.V. Eester, E. Lerche, T. Wauters, J. Ongena, Potential of ion cyclotron resonance frequency current drive via fast waves in DEMO, Plasma Phys. Control. Fusion 24 (2) (2015) 025014.

[3] Y. Kazakov, J. Ongena, J.C. Wright, S.J. Wukitch, E. Lerche, M.J. Mantsinen, D.V. Eester, T. Craciunescu, V. Kiptily, Y.-M. Lin, M. Nocente, F. Nabais, M.F.F. Nave, Y. Baranov, J. Bielecki, R. Bilato, V. Bobkov, K. Crombé, A. Czarnecka, J.M. Faustin, R. Felton, M. Fitzgerald, D. Gallart, L. Giacomelli, T. Golfinopoulos, A.E. Hubbard, P. Jacquet, T. Johnson, M. Lennholm, T. Loarer, M. Porkolab, S.E. Sharapov, D.F. Valca?rcel, M. Schoor, H. Weisen, Efficient generation of energetic ions in multi-ion plasmas by radio-frequency heating, Nat. Phys. 13 (2017) 973–978.

[4] M. Bure, J.J. Jacquinot, K. Lawson, M.F. Stamp, H.P. Summers, D.A. D'Ippolito, J.R. Myra, Impurity release from the ICRF antenna screens in JET, Plasma Phys. Control. Fusion 33 (1991) 937–967.

[5] C. Gal, J. Rice, M. Reinke, Y. Lin, S. Wukitch, L. Delgad0-Aparicio, E. Marmar, A.C.-M. Team (Eds.), ICRF induced argon pumpout in H-D plasmas at alcator C-mod, in: AIP Conf. Proc., Vol. 1, no. TP8.017, October, 2014, APS Division of Plasma Physics Meeting(2014) TP8.01.

[6] G. Federici, R. Kemp, D. Ward, C. Bachmann, T. Franke, S. Gonzalez, C. Lowry, M. Gadomska, J. Harman, B. Meszaros, C. Morlock, F. Romanelli, R. Wenninger, Overview of EU-DEMO design and R&D activities, Fusion Eng. Des. 89 (2014) 882–889.

[7] A. Garcia, J.-M. Noterdaeme, U. Fischer, J. Dies, Effect on tritium breeding ratio due to a distributed ICRF antenna in a DEMO reactor, Fusion Eng. Desgin 112 (2016) 298–302.

[8] G. Bosia, Low power density ion cyclotron arrays for fusion reactors, Fusion Eng. Desgin 92 (2015) 8–15.

[9] R. Ragona, A. Messiaen, J. Ongena, D.V. Eester, M.V. Schoor, J.-M. Berrnard, J. Hillairet, J.M. Noterdaeme, A travelling wave array system as solution for the ion cyclotron resonance frequencies heating of DEMO, Nucl. Fusion 60 (2020) 016027.

[10] M.Q. Tran, P. Agostinetti, G. Aiello, K. Avramidis, B. Baiocchi, M. Barbisan, V. Bobkov, S. Briefi, A. Bruschi, R. Chavana, I. Chelis, C. Day, R. Delogu, B. Ell, F. Fanale, A. Fassina, U. Fantz, H. Faugel, L. Figini, D. Fiorucci, R. Friedl, T. Franke, G. Gantenbein, S. Garavaglia, G. Granucci, S. Hanke, J.-P. Hogge, C. Hopf, A. Kostic, S. Illy, Z. Ioannidis, et al., Status and future development of heating and current drive for the EU DEMO, Fusion Eng. Des. 180 (2022) 113159.

[11] H. Kasahara, T. Seki, K. Saito, R. Seki, R. Kumazawa, Y. Yoshimura, S. Kubo, T. Shimozuma, H. Igami, H. Takahashi, K. Nagasaki, Y. Ueda, M. Tokitani, N. Ashikawa, M. Shoji, T. Wakatsuki, S. Kamio, H. Tsuchiya, S. Yoshimura, N. Tamura, C. Suzuki, H. Yamada, T. Mutoh, Development of steady-state operation using ion cyclotron heating in the large helical device, Phys. Plasmas 21 (2014) 061505.

[12] M.L. Garrett, S.J. Wukitch, P. Koert, D.G. Whyte, Magnetic field-aligned ICRF antenna to minimize RF sheaths*, Bull. Am. Phys. Soc. (2011).

[13] V. Bobkov, R. Bilato, L. Colas, R. Dux, E. Faudot, H. Faugel, H. Funfgelder, A. Herrmann, J. Jacquot, A. Kallenbach, D. Milanesio, R. Maggiora, R. Neu, J.-M. Noterdaeme, R. Ochoukov, T. Putterich, W. Tierens, W. Zhang, the ASDEX Upgrade Team, the EURO fusion MST1 Team, Characterization of 3-strap antennas in ASDEX upgrade, EPJ Web Conf. 157 (2017) 03005.

[14] R. Kumazawa, T. Mutoh, T. Seki, T. Watari, S. Masuda, F. Shimpo, K. Nishimura, T. Kuroda, D. Rasmussen, R.H. Goulding, M.D. Carter, D.J. Hoffman, Development of folded waveguide antenna for ICRF heating in the large helical device, Fusion Eng. Desgin 26 (1995) 395–403.

[15] K. Crombea, V. Kyrytsyab, R. Kochb, D.V. Eesterb (Eds.), Simulations of ICRF Antenna Near-Fields in Dielectric Media and Cold Plasmas with COMSOL, Vol. 97, 2011.

[16] K. Saito, T. Seki, H. Kasahara, R. Seki, S. Kamio, G. Nomura, T. Mutoh, Performance of impedance transformer for high-power ICRF heating in LHD, J. Phys. Conf. Ser. 823 (2017) 012007.

[17] S.J. Wukitch, R. Bivin, P. Bonoli, J. Goetz, J. Hosea, Y. Lin, M. Porkolab, I. Htchinson, E. Marmar, G. Schililing, J. Wilson, Performance of a compact four-strap fast wave antenna, in: FEC(Lyon), France, FT/P1-14, 2003.

[18] T. Goto, J. Miyazawa, H. Tamura, T. Tanaka, S. Hamaguchi, N. Yanagi, A. Sagara, the FFHR Design Group, Design window analysis for the helical DEMO reactor FFHR-D1, Plasma Fusion Res. 7 (2012) 2405084.

[19] R.C. Wolf, C.D. Beidler, R. Burhenn, J. Geiger, M. Hirsch, J. Kisslinger, H. Maasberg, A. Weller, A. Werner, the Wendelstein 7-X Team, From Wendelstein 7-X to a stellarator reactor, Plasma Fusion Res. 5 (2010) S1011.